Cancer Research

Pharmacological Inhibition of the Histone Lysine Demethylase KDM1A Suppresses the Growth of Multiple Acute Myeloid Leukemia Subtypes

John P. McGrath[1], Kaylyn E. Williamson[1], Srividya Balasubramanian[1], Shobu Odate[1], Shilpi Arora[1], Charlie Hatton[1], Thomas M. Edwards[1], Thomas O'Brien[2], Steven Magnuson[3], David Stokoe[4], Danette L. Daniels[5], Barbara M. Bryant[1], and Patrick Trojer[1]

Abstract

Lysine-specific demethylase 1 (KDM1A) is a transcriptional coregulator that can function in both the activation and repression of gene expression, depending upon context. KDM1A plays an important role in hematopoiesis and was identified as a dependency factor in leukemia stem cell populations. Therefore, we investigated the consequences of inhibiting KDM1A in a panel of cell lines representing all acute myelogenous leukemia (AML) subtypes using selective, reversible and irreversible KDM1A small-molecule inhibitors. Cell models of AML, CML, and T-ALL were potently affected by KDM1A inhibition, and cells bearing *RUNX1-RUNX1T1* (*AML1-ETO*) translocations were especially among the most sensitive. RNAi-mediated silencing of KDM1A also effectively suppressed growth of *RUNX1-RUNX1T1*–containing cell lines. Furthermore, pharmacologic inhibition of KDM1A resulted in complete abrogation of tumor growth in an AML xenograft model harboring *RUNX1–RUNX1T1* translocations. We unexpectedly found that KDM1A-targeting compounds not only inhibited the catalytic activity of the enzyme, but evicted KDM1A from target genes. Accordingly, compound-mediated KDM1A eviction was associated with elevated levels of local histone H3 lysine 4 dimethylation, and increased target gene expression, which was further accompanied by cellular differentiation and induction of cell death. Finally, our finding that KDM1A inhibitors effectively synergize with multiple conventional as well as candidate anti-AML agents affords a framework for potential future clinical application. *Cancer Res; 76(7); 1975–88. ©2016 AACR.*

Introduction

Posttranslational modifications of histone proteins contribute to the dynamic alteration of chromatin structure, and thus impact gene expression in normal and malignant cells. Modulation of histone lysine methylation patterns by histone lysine methyltransferases (KMT) and demethylases (KDM) has been recognized as a gene regulatory pathway that is frequently targeted in cancer (1). Cancer genomic sequencing campaigns have led to the identification of recurrent genomic abnormalities in genes that encode for chromatin-modifying enzymes (2–6), supporting the concept that cancer cells utilize the manipulation of chromatin structure as one means to invoke transcriptional programs that prevent differentiation and promote proliferation. The emergence of individual KMTs and KDMs as candidate oncology targets has spurred significant drug discovery efforts with the goal to identify small-molecule inhibitors of these enzymes for cancer therapeutic applications (1, 7, 8).

Lysine demethylase 1 (KDM1A, LSD1, AOF2, BHC110) belongs to the amine oxidase family of KDMs and utilizes FAD as a cofactor to remove mono- and di-methyl groups from histone H3 lysine 4 (H3K4; ref. 9) and H3K9 (10, 11). KDM1A is a component of a multisubunit complex that, depending on context, functions in transcriptional activation or repression. Core components include RCOR1 (CoREST) that is required for KDM1A to demethylate nucleosomal substrates (12, 13), PHF21A (BHC80) that recognizes unmethylated histone H3 lysine 4 (14), and HMG20B (BRAF35) that recognizes DNA (15). Initially, KDM1A's role in transcription was ascribed to promoter-proximal modulation of chromatin structure, but recent evidence suggests that KDM1A also functions in decommissioning of enhancers (16). KDM1A is essential for embryonic development (17, 18), and is required for hematopoietic cell lineage determination (19).

KDM1A is significantly overexpressed in a number of hematologic malignancies (20, 21) and lymphoid neoplasms (22). In acute myelogenous leukemia (AML), KDM1A is among the most highly expressed genes in leukemia stem cell-enriched populations derived from different primary AML subtypes (23). KDM1A was shown to cooperate with the oncogenic fusion protein MLL-AF9 to sustain leukemic stem cells (24). Depletion of KDM1A by RNAi and pharmacologic inhibition of KDM1A induced differentiation in murine and primary human MLL-AF9 leukemia cells. Moreover, KDM1A inhibition reactivated the retinoic acid signaling pathway in certain AML subtypes, rendering these cells sensitive to all-*trans*-retinoic acid (ATRA) treatment (25). The scope of

[1]Biology, Constellation Pharmaceuticals, Inc., Cambridge, Massachusetts. [2]Oncology, Genentech Inc., South San Francisco, California. [3]Drug Metabolism and Pharmacokinetics, Genentech Inc., South San Francisco, California. [4]Molecular Biology, Genentech Inc., South San Francisco, California. [5]Promega Corporation, Madison, Wisconsin.

Note: Supplementary data for this article are available at Cancer Research Online (http://cancerres.aacrjournals.org/).

Corresponding Author: Patrick Trojer, Constellation Pharmaceuticals, Inc., 215 First Street, Cambridge, MA 02142, USA. Phone: 617-714-0555; Fax: 617-577-0472; E-mail: patrick.trojer@constellationpharma.com

doi: 10.1158/0008-5472.CAN-15-2333

KDM1A dependencies is as yet unclear (26), and an understanding of the mechanistic consequences of KDM1A inhibition in a disease-relevant context is still lacking.

Here, we show that KDM1A dependencies exist across cell lines representing all AML subtypes [French-American-British (FAB) M1-M6 classification] and are also observed in cells derived from additional hematologic malignancies. We demonstrate that KDM1A inhibitors effectively suppress the growth of *RUNX1-RUNX1T1* translocated AML cells *in vitro* and *in vivo* and determine the molecular consequences of KDM1A inhibition in *RUNX1-RUNX1T1* leukemias. Finally, we explored the potential of KDM1A inhibitors to synergize with other chemotherapeutic and targeted agents in the treatment of AML and beyond.

Materials and Methods

Cell lines

A collection of 50 hematologic cell lines investigated in this study is summarized in Supplementary Table S1. The cell lines were obtained either through the ATCC or DSMZ. The identity of the cell lines was authenticated by short tandem repeat (STR) profiling and cultures were also tested for the presence of Mycoplasma (IDEXX Bioresearch) before the initiation of this study. Cell lines were maintained according to the instructions provided by the respective repositories.

Antibodies

Antibodies targeting the following proteins were used: KDM1A (CST, #2184, Bethyl, A300-215A), histone H3 (CST, #3638), dimethyl H3K4 (Millipore, 07-030), trimethyl H3K4 (Abcam, ab8580), dimethyl H3K9 (Abcam, ab1220), RCOR1 (Millipore, 07-455), PHF21A (Bethyl, A303-603A), HMG20B (Bethyl, A301-097A), RUNX1 (Abcam, ab23980), RUNX1T1 (Santa Cruz Biotechnology, sc-9737), RUNX1-RUNX1T1 (Diagenode, C15310197), lamin B1 (Abcam, ab16408), vinculin (Sigma, V9264), IgG (Abcam, ab46540), DyLight conjugated goat anti-mouse (ThermoFisher, 35518), and anti-rabbit (ThermoFisher, 35571) IgG secondary antibodies were used for Western blot detection on an Odyssey CLx Infrared Imaging System (LI-COR Biotechnology). For cell surface marker analysis by flow cytometry, the antibodies included: CD86 (B7-2)-PE (eBiosciences, 12-0869), CD11b–FITC (eBiosciences, 11-0118), CD11c-APC (eBioscience, 17-0116), as well as the isotype-matched control antibodies: mouse IgG2b, kappa-PE (eBiosciences, 12-4732), mouse IgG1, kappa-FITC (eBiosciences, 11-4714), and mouse IgG1, kappa-APC (eBiosciences, 17-4714).

Cell proliferation assays

Cells were plated at 10,000 cells per well in 96-well tissue culture dishes containing tool compounds arrayed in triplicate in a semi-automated fashion (compounds dispensed with Echo 555 Liquid Handler, Labcyte) using a 10-point dose titration, ranging from 0 to 10 μmol/L with 4-fold dilutions, and split every fourth day at a ratio to reestablish 10,000 cells/well density for DMSO-treated controls. Relative cell numbers were assessed by Cell Titer-Glo luminescent cell viability assay (Promega) using an EnVision Multilabel Plate Reader (PerkinElmer). GraphPad Prism 6 (GraphPad Software, Inc.) was used for curve fitting and determination of GI_{50} values. For details, see Supplementary Methods.

Cell cycle and apoptosis

Cells were plated in 96-well plates and treated with doses ranging from 10 μmol/L to 0 μmol/L (DMSO) across 4-fold dilutions of the respective inhibitor. The cells were split on days 4, 8, and 12 to maintain logarithmic growth and collected upon splitting for analysis. For cell-cycle analysis, cells were fixed in 70% ice-cold ethanol overnight at 4°C. The fixed cells were resuspended in propidium iodide (PI) staining buffer (50 μg/mL PI, 10 μg/mL RNase in PBS), and then incubated for 1 hour at room temperature in total darkness. The cellular DNA content was assessed on Guava EasyCyte cytometer (Millipore). The percentage of cells in the different cell-cycle phases were determined by analysis using the Guava CytoSoft software package (Millipore). For analysis of apoptosis, unfixed cells were stained with PI and Annexin-FITC using the TACS Annexin V Kit (Trevigen) following the instructions provided. Data were acquired on a Guava EasyCyte and the percentage of cells undergoing apoptosis was calculated using Guava CytoSoft 5.3.1 program.

RNAi

Stable knockdown of KDM1A was achieved using lentiviral-based shRNA vectors (Cellecta). Production and processing of lentiviral stocks were carried out following standard protocols. A set of two nonoverlapping shRNAs and a nontargeting control shRNA (NTC) shRNA was selected for use in all experiments. Cells were transduced using lentiviral vectors expressing the NTC shRNA or KDM1A-targeting shRNAs at an MOI of 2 using a spin-infection protocol where virus was added to 3×10^5 cells in each well of a 6-well dish in media supplemented with 8 μg/mL Polybrene (Boston BioProducts) and cultures were centrifuged at 1,000 × g for 1 hour. Media were changed 48 hours later with or without the addition of puromycin (2 μg/mL). For cells under puromycin selection, after 72 hours cells were plated at equal densities and monitored for cell proliferation via CellTiterGlo (CTG, Promega) every 4 days and target gene transcript levels assessed by qRT-PCR. For cells not placed under puromycin selection, cells were monitored every 4 days for % GFP-positive cells via flow cytometry using a Guava EasyCyte (Millipore) and CytoSoft 5.3.1 software (Millipore).

Gene expression

Cells were pelleted and RNA isolated using an RNeasy Kit (Qiagen). qRT-PCR analysis was carried out as described previously (27). The *LY96* mRNA induction was quantified using the QuantiGene 2.0 system (Affymetrix). RNA-sequencing from total RNA samples was carried out using the services of Ocean Ridge Biosciences. For details, see Supplementary Methods. RNA-seq data have been submitted to GEO (GSE71739).

NanoBRET assay

Experiments were carried out as described previously (27). For details, see Supplementary Methods.

Chromatin immunoprecipitation and ChIP-sequencing

Experiments in Kasumi-1 and SKNO-1 cells were carried out as described previously (27). For a detailed description of the chromatin immunoprecipitation (ChIP) procedure and ChIP-sequencing (seq) data analysis, see Supplementary Methods. ChIP-seq data have been submitted to GEO (GSE71740).

***In vivo* experiments**

CB-17 SCID mice were inoculated subcutaneously at the right flank with Kasumi-1 cells (1×10^7) in 0.2 mL of PBS with Matrigel (1:1). Treatment was started when the average tumor volume reached approximately 120 mm^3. Each group consisted of 10 tumor-bearing mice. Tumor-bearing mice were treated with one of the following regimens: vehicle (0.5% methylcellulose + 0.2% Tween 80) or RN-1 at 1 mg/kg QD or RN-1 at 17.5 mg/kg QW. Tumor size was measured three times a week using a caliper, and the tumor volume (V) was expressed in mm^3 using the formula: $V = 0.5a \times b^2$ where "a" and "b" were the long and short diameters of the tumor, respectively. The mice were weighed every day. TGI% was calculated according to the following equation: TGI (%) = [1-(T1-T0)/(V1-V0)] × 100, where V1- mean tumor volume of control mice at time t; T1 -mean tumor volume of treated mice at time t; V0-mean tumor volume of control mice at time 0; T0-mean tumor volume of treated mice at time 0. Studies continued until the tumor volume reached 2,000 mm^3 as per IACUC guidelines. At study termination, the tumor samples were collected for pharmacokinetic and gene expression studies. For pharmacodynamic analysis, animals were dosed according to the protocol for a final time and blood and tumor were collected at designed time points for assessment.

Results

KDM1A inhibitors elicit phenotypic responses in cell models of various hematologic malignancies

To explore potential KDM1A dependencies in hematologic malignancies, we used the published cyclopropylamine-based irreversible KDM1A inhibitor RN-1 (28). Consistent with previous data, RN-1 is a potent inhibitor of KDM1A but not of the closely related demethylase enzyme LSD2 (KDM1B, AOF1) in enzymatic assays (Supplementary Fig. S1A). We devised a cellular thermal shift assay (CETSA; ref. 29) for KDM1A to determine the extent of cellular target engagement. RN-1 thermo-stabilized endogenous KDM1A protein at 52°C to 56°C, conditions that clearly caused thermally induced KDM1A denaturation/precipitation in DMSO-treated control cells (Supplementary Fig. S2A). Subsequent CETSA experiments demonstrated that RN-1 thermo-stabilized KDM1A in a dose-dependent manner (Supplementary Fig. S2B), indicating that the compound directly engages its target.

Having qualified RN-1 as a suitable tool compound, we carried out long-term (12 day) growth assays across a panel of 50 hematologic cancer cell lines in the presence of DMSO or various concentrations of RN-1. The growth of all tested AML cell lines regardless of subtype, both CML cell lines and a number of T-ALL lines were potently affected by RN-1. In contrast, none of the B-ALL and diffuse large B-cell lymphoma cell lines tested showed any growth defect upon treatment (Fig. 1A). All observed cell viability defects were dose- and time dependent (Fig. 1A, see examples on the right), with multiple days of treatment required to elicit the maximal effects, suggesting that the response timing of downstream molecular consequences of KDM1A inhibition is slow. Phenotypic responses after 12 days of dosing were varied with sensitive cell lines showing maximal growth inhibition ranging from 40% to 100%. The entire cell population of complete responder cell lines was eliminated by RN-1, while sensitive cell lines exhibiting <70% reduction in cell number over the course of the 12-day treatment were referred to as "partial" responders (Fig. 1A, see example on the right). Cell lines that did not exhibit any growth defect after a 12-day treatment were determined as "non-responders" (Fig. 1A, see example on the right). The partial phenotype observed in some AML cell lines may indicate that KDM1A is required only in a subpopulation of cells or that a mixture of cytotoxic and cytostatic responses is obtained upon compound treatment. Several of these AML cell lines were increasingly growth suppressed when the treatment period was extended or when tested in a clonogenic colony formation assay (Supplementary Fig. S3A–S3C). Strong and complete responses were most evident in the M2 AML subtype, which includes the *RUNX1-RUNX1T1* rearranged leukemias, as well as in the M6-M7 subtypes that constitute acute megakaryoblastic and erythroid leukemias (Fig. 1A).

To corroborate these cell viability data, we took advantage of another recently disclosed KDM1A inhibitor (30). GSK690 is structurally distinct from RN-1, lacking the tranylcypromine moiety and was described as a reversible inhibitor. GSK690 also potently and selectively inhibits KDM1A in biochemical and cellular assays and directly interacts with KDM1A, as indicated by the observed thermal stabilization of the protein (Supplementary Figs. S1B and S2A and S2C). The cell growth defects across the hematologic cancer cell panel upon GSK690 treatment paralleled those observed with RN-1 (Fig. 1B), suggesting that these phenotypic effects are indeed caused through inhibition of KDM1A demethylase activity.

AML models harboring *RUNX1-RUNX1T1* translocations are dependent on KDM1A

The *t*(8;21) chromosome translocation fuses the transcription factors RUNX1 (AML1, CBFA2) and RUNX1T1 (ETO, ZMYND2). The resultant RUNX1-RUNX1T1 fusion gene product was found to drive leukemic transformation, prevent differentiation, and promote oncogenic programs (31–33). RUNX1-RUNX1T1 leukemias represent approximately 10% to 15% of adult AML (34). Treatment with the irreversible KDM1A inhibitor RN-1 caused a dose and time-dependent viability defect in Kasumi-1 (Fig. 2A) and SKNO-1 (Supplementary Fig. S4A), both AML cell models with *RUNX1-RUNX1T1* translocations. Similarly, both cell lines were potently affected by the reversible KDM1A inhibitor GSK690 (Fig. 2A and Supplementary Fig. S4A). We discovered that a positional isomer of GSK690, in which the nitrile and methyl groups are switched, is a significantly less potent KDM1A inhibitor in enzymatic (Supplementary Fig. S1C) and cellular target engagement assays (Supplementary Fig. S2A and S2D). This regioisomer, termed GSK690*, has similar physicochemical properties as GSK690, and thus serves as a useful tool to discern on-target from off-target activities. As expected, GSK690* did not elicit potent cell viability defects in Kasumi-1 and SKNO-1 cells (Fig. 2A and Supplementary Fig. S4A), suggesting that the phenotypic effects caused by GSK690 and RN-1 are mediated through compound on-target activity. KDM1A inhibition increased the sub-G_1 cell population (Fig. 2B and Supplementary Fig. S4B) and induced apoptosis (Fig. 2C and Supplementary Fig. S4C). Moreover, KDM1A inhibitors promoted myeloid differentiation in RUNX1-RUNX1T1 leukemias, as measured by the dose-dependent increase in the levels of the CD86, CD11B, and CD11C cell surface markers (Fig. 2D and Supplementary Fig. S4D).

A

Cancer type		Cell line	RN-1 GI_{50}
AML	1	HL-60 (M2)	0.014
	2	Kasumi-1 (M2)	0.004
	3	SKNO-1 (M2)	0.011
	4	NB-4 (M3)	Partial
	5	PL-21 (M3)	Partial
	6	OCI-AML2 (M4)	0.038
	7	OCI-AML3 (M4)	Partial
	8	OCI-AML5 (M4)	Partial
	9	ME-1 (M4)	3.494
	10	MUTZ-8 (M4)	<0.02
	11	ML-2 (M4)	Partial
	12	NOMO-1	Partial
	13	MOLM-13	Partial
	14	SKM-1 (M5)	Partial
	15	MV4-11 (M5)	0.017
	16	THP-1 (M5)	Partial
	17	U937 (M5)	Partial
	18	OCI-M1 (M6)	0.053
	19	OCI-M2 (M6)	0.074
	20	HEL (M6)	0.028
	21	KG-1 (M7)	0.748
	22	SET2 (M7)	0.012
	23	UKE-1 (M7)	< 0.02
	24	MKPL-1 (M7)	0.009
	25	EOL-1	<0.02
CML	26	KU812F	<0.02
	27	K-562	0.08
T-ALL	28	PEER	0.04
	29	RPMI-8402	0.023
	30	CCRF-HSB-2	0.107
	31	Loucy	Partial
	32	MOLT-4	Partial
	33	Jurkat	>10
	34	MOLT-16	>10
	35	CCRF-CEM	>10
	36	TALL-1	>10
B-ALL	37	ROS-50	Partial
	38	Reh	>10
	39	RS4;11	>10
	40	KOPN-8	>10
	41	NALM-6	>10
	42	SUP-B15	>10
	43	TANOUE	>10
	44	VAL	>10
DLBCL	45	FARAGE	>10
	46	SU-DHL-4	>10
	47	OCI-LY1	>10
	48	OCI-LY7	>10
	49	U-2973	>10
	50	TMD-8	>10

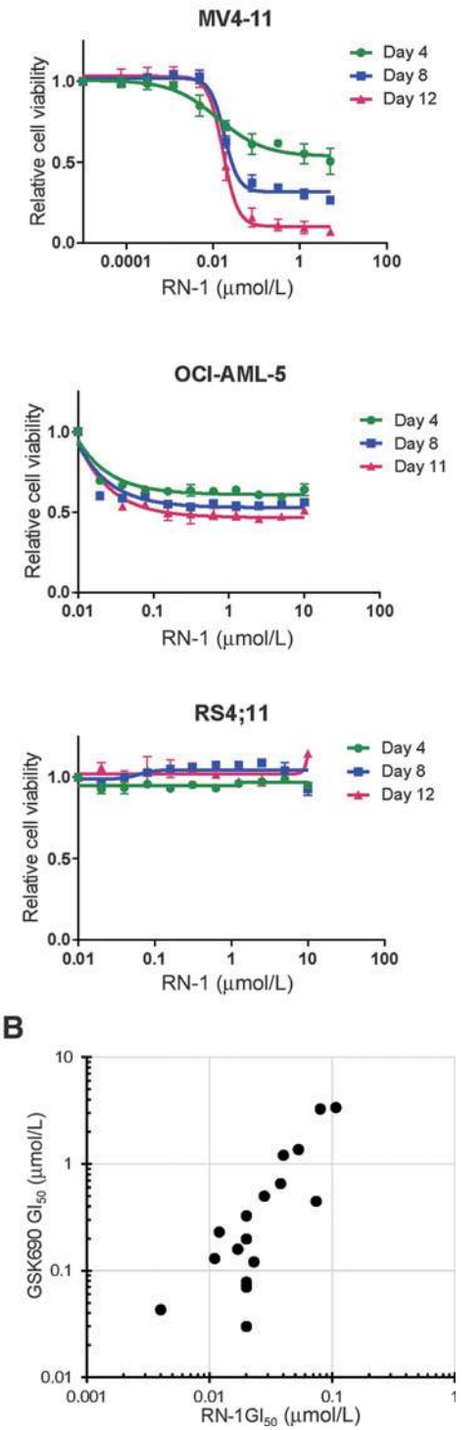

Figure 1.
KDM1A inhibition across a panel of cell lines representing various hematologic malignancies. A, effects of the KDM1A inhibitor RN-1 on growth of AML (#1-25), CML (#26-27), B-ALL (#28-36), T-ALL (#37-44), and diffuse large B-cell lymphoma (#45-50) cell lines. Half-maximal growth inhibitory concentration (GI_{50}) values were determined on day 12 of treatment. "Partial" designation was assigned to responder cell lines showing less than 70% cell killing by day 12 of treatment. Data represent the mean of triplicate experiments. Type of hematologic malignancy, cell line name, and FAB classification (for AML cell lines) are indicated. Growth profiles reflecting the three types of responses observed in AML cell models upon KDM1A inhibition are shown on the right: top, MV4-11, a complete response; middle, OCI-AML5, a partial response; bottom, RS4;11, a non-response. Cells were passaged every 4 days and the number of viable cells was determined at each split. Data represent the mean of three independent experiments carried out in duplicate ±SD. B, similarity in the cellular responses observed for the irreversible KDM1A inhibitor RN-1 and the reversible KDM1A inhibitor GSK690. GI_{50} values determined for complete responding cell lines were plotted for each of the two KDM1A inhibitors. Data represent the mean GI_{50} value at day 12 from triplicate experiments.

We used RNAi as an orthogonal approach to demonstrate that RUNX1-RUNX1T1–containing AML cell lines are dependent on KDM1A. In both Kasumi-1 and SKNO-1 cells, multiple KDM1A-specific shRNAs, but not control shRNAs, effectively reduced KDM1A transcript and protein levels and caused substantial cell viability defects (Fig. 2E and F and Supplementary Fig. S4E and S4F). Consistent with compound-mediated effects, KDM1A-targeted shRNAs also induced the expression of differentiation markers such as LY96, CD86, CD11B, and CD11C (Fig. 2G and Supplementary Fig. S4G). Our data suggest that KDM1A is required for the *in vitro* growth of RUNX1-RUNX1T1–containing AML cell lines.

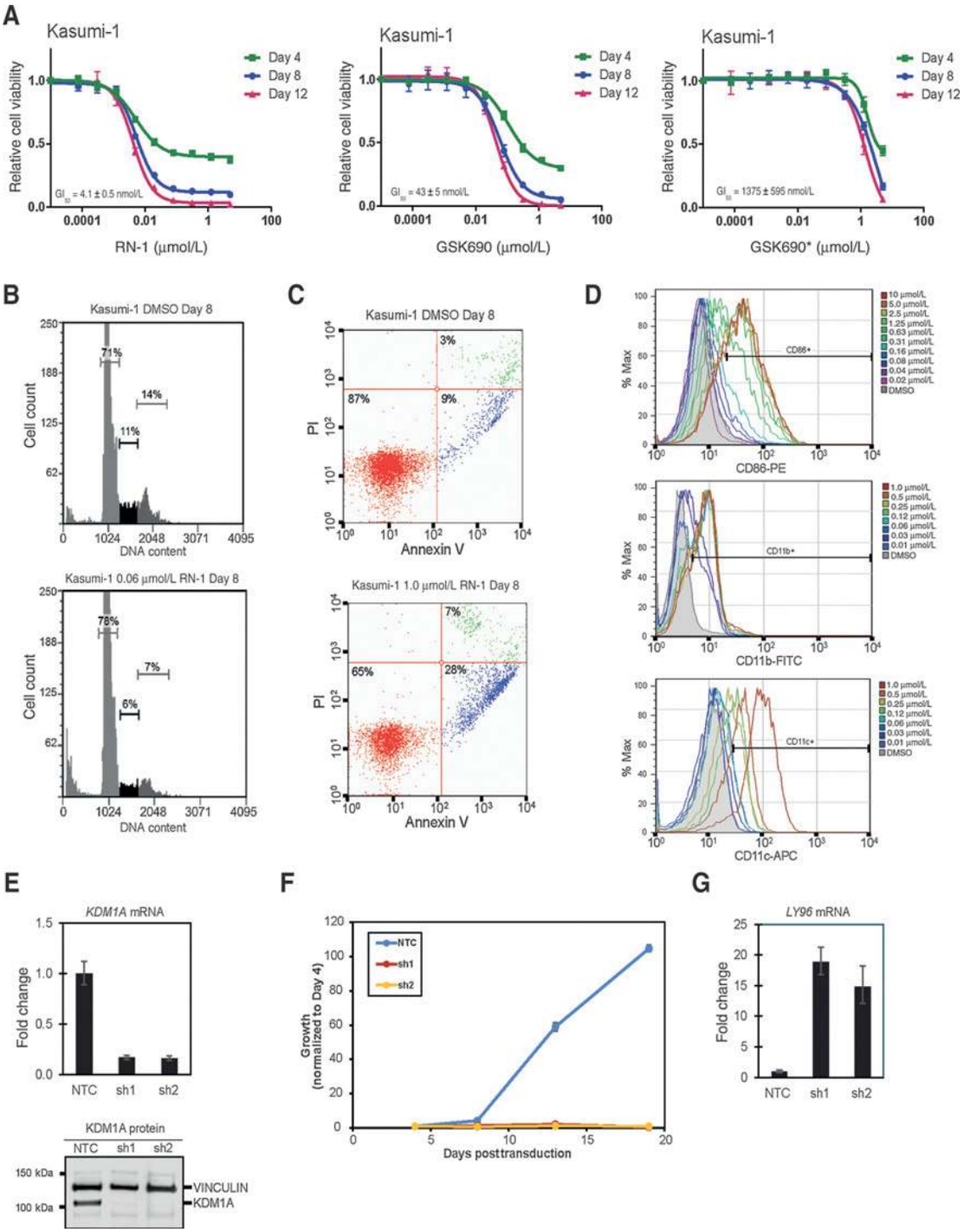

Figure 2.

KDM1A inhibition effects on the RUNX1-RUNXT1 cell line Kasumi-1. A, growth inhibition curves for Kasumi-1 cells treated with the irreversible KDM1A inhibitor RN-1, the reversible KDM1A inhibitor GSK690, and the less potent position isomer of the reversible inhibitor, GSK690*. Data represent the mean of three independent experiments carried out in duplicate ±SD. B, treatment of Kasumi-1 cells with RN-1 leads to a depletion of cells in S/G_2 phase of the cell cycle, concomitant with an increase in cell numbers in the G_1 and sub-G_1 compartments as determined by analysis using a Guava EasyCyte flow cytometer. C, Annexin-V (Ann-V) and PI staining profile showing Kasumi-1 cells undergoing apoptosis following treatment with RN-1 for 8 days. Red quadrant represents live cells that show no staining with either Annexin-V or PI; bottom right (blue) area shows cells that are in early apoptosis, Annexin-V–positive and PI negative/low, while the top right green quadrant reflects cells that are in late apoptosis. Debris and dead cells were gated out to generate this plot. D, dose-dependent induction of the differentiation markers CD86, CD11B, and CD11C in Kasumi-1 cells upon treatment with RN-1 for 6 days, as measured on a BD FACS Calibur cytometer following staining with the relevant fluorophore-conjugated antibodies. E, KDM1A targeted shRNAs effectively reduce KDM1A transcript and protein levels in Kasumi-1 cells. F, RNAi-mediated knockdown of KDM1A inhibits the growth of Kasumi-1 cells in culture. G, RNAi-mediated knockdown of KDM1A induces expression of the *LY96* gene.

KDM1A inhibitors are efficacious in Kasumi-1 xenografts

To explore KDM1A dependency in RUNX1-RUNX1T1-containing leukemias *in vivo*, we established Kasumi-1 xenografts in SCID mice. Once daily administration of RN-1 at 1 mg/kg completely abolished tumor growth (Fig. 3A). This dose was well tolerated since no impact on body weight was observed. Given that KDM1A is essential for hematopoiesis (19), the peripheral blood of RN-1–treated animals was analyzed for potential detrimental effects. There were no significant changes in abundance detected in any population of the various blood cell types over the course of treatment (Supplementary Table S1), suggesting that there is a sufficient therapeutic window to separate therapeutic effects from anticipated hematologic toxicity. Interestingly, a single dose of 17.5 mg/kg was sufficient to suppress tumor growth for 9 days (Fig. 3A), suggesting that intermittent dosing schedules may be possible and useful for irreversible KDM1A inhibitors sharing similar pharmacokinetic properties. The expression level of the cell surface protein CD86 was previously described as a surrogate biomarker for KDM1A inhibition (35). Consistently, we detected a significant induction of *CD86* expression in treated tumors (Fig. 3B). We also identified the gene for lymphocyte antigen *LY96* as a direct KDM1A target (see data below) and detected significant increases in *LY96* steady state transcript levels in RN-1–treated tumors (Fig. 3B, right), thus establishing a correlation between administered dose, target inhibition, and tumor growth.

KDM1A controls a specific gene expression program in RUNX1-RUNX1T1–containing leukemias

To investigate the transcriptional changes caused by KDM1A inhibition, we performed RNA-sequencing in Kasumi-1, SKNO-1 cell models (*RUNX1-RUNX1T1* translocation), and MV4-11 (*MLL-AF4* translocation) cells in the absence or presence of the KDM1A inhibitors RN-1 and GSK690. Gene expression changes caused by both chemotypes were very similar (Fig. 4A). Treatment with RN-1 for 72 hours resulted in a number of genes that were consistently and significantly altered (>2-fold change, $P < 0.05$) in each cell line: 215 in Kasumi-1, 159 in SKNO-1, and 375 in MV4-11. The majority of transcriptionally altered genes were distinct in each cell line (Fig. 4B). Genes consistently altered by RN-1 treatment in all three cell lines included myeloid differentiation markers, such as *CD86*, *CD53*, *LY96*, *LYZ*, *ITGAM* (CD11B), *ITGAX* (CD11C), *SELL* (CD62L), *PLAUR* (CD87), and *EFNA4* (Fig. 4B and C). Murine leukemia models with *MLL-AF9* translocations were previously shown to elicit gene expression changes upon *Kdm1a* knockdown with the majority of transcriptionally altered genes being downregulated (24). To the contrary, we

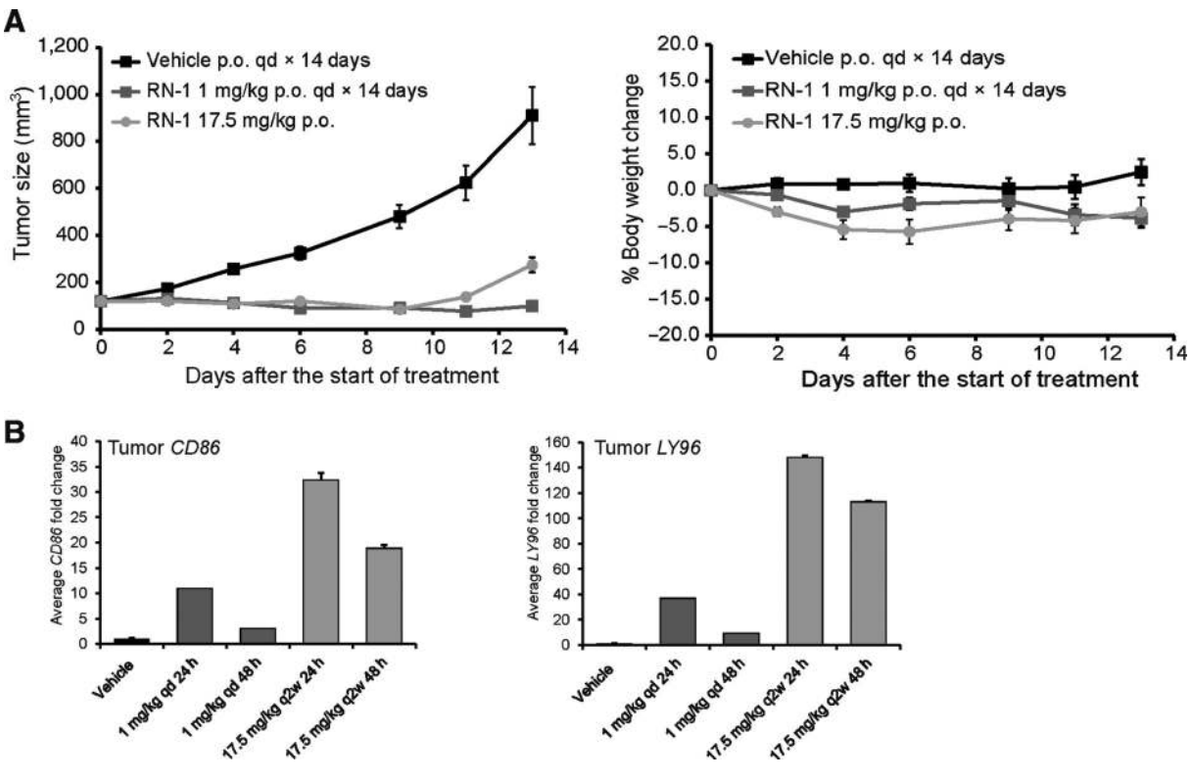

Figure 3.

KDM1A inhibition abrogates growth of Kasumi-1 xenografts. A, tumor growth curves (left) and body weight changes (right) of Kasumi-1 xenografts treated with the indicated doses of RN-1. CB-17 SCID mice were inoculated subcutaneously at the right flank with 1×10^7 Kasumi-1 cells for tumor development. Treatment with vehicle (0.5% MC + 0.2% Tween80) and RN-1 via oral gavage (p.o.) was initiated at an average tumor size of 120 mm^3 ($n = 10$ per cohort). Once daily (qd) administration of 1 mg/kg RN-1 proved efficacious in preventing tumor growth. A single dose of 17.5 mg/kg of RN-1 was efficacious for 9 days before evidence of tumor growth was detected. Data are presented as the mean tumor size ±SEM. None of the dose regimen led to a significant (≥10%) decrease in body weight. Data are presented as the mean body weight ±SEM. B, dose-dependent induction of *CD86* (left) and *LY96* (right) gene expression in xenografts ($n = 4$ per cohort) following RN-1 treatment. RNA extracted from tumor samples at 24 and 48 hours post the last dose and analyzed by TaqMan qRT-PCR. Data represent the mean of all analyzed xenograft samples per cohort with triplicate qPCR experiments ±SEM.

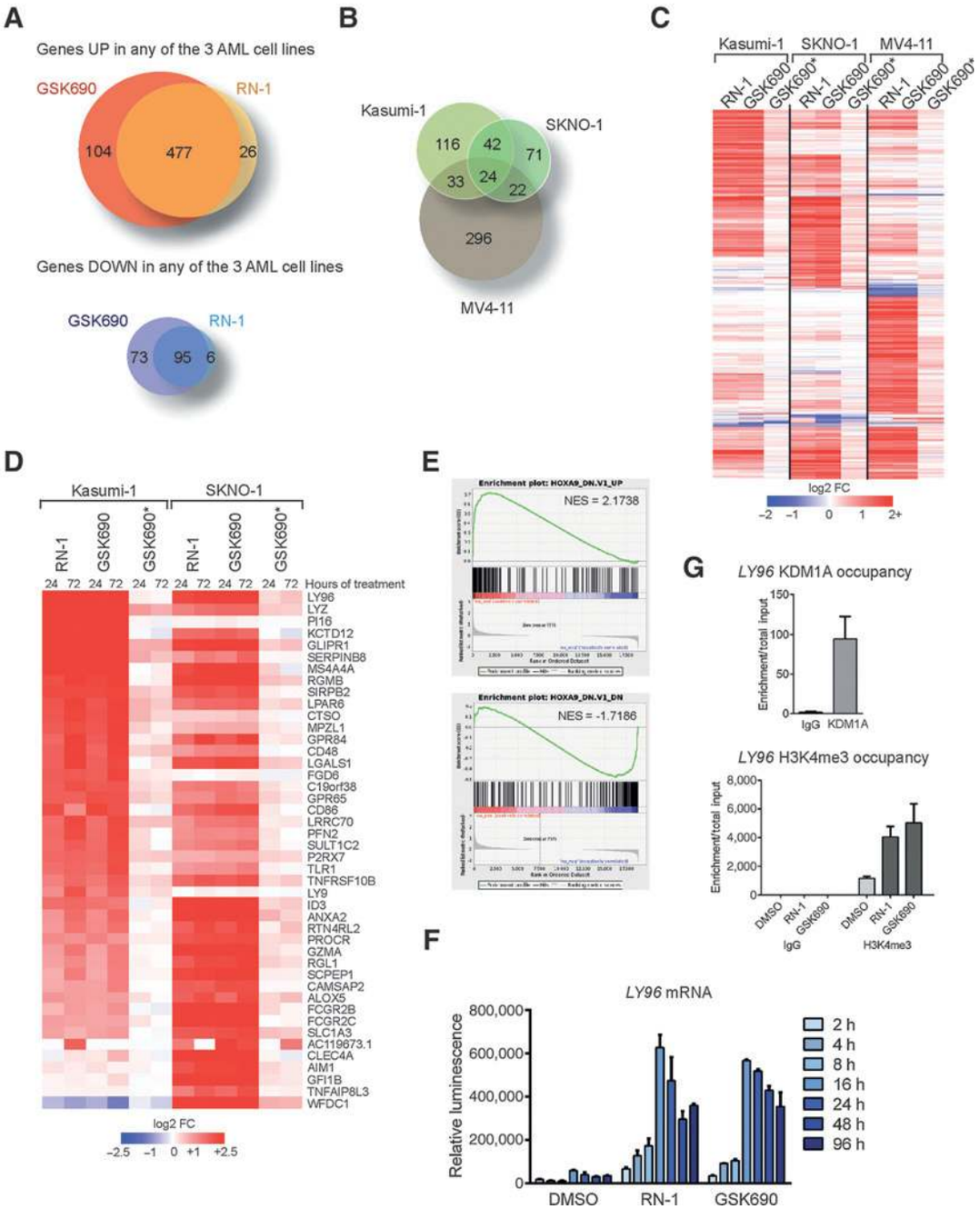

Figure 4.

KDM1A catalytic activity is required to control a specific gene expression program in RUNX1-RUNXT1 leukemias. A, RNA sequencing was performed in Kasumi-1, SKNO-1, and MV4-11 cells treated with DMSO, RN-1, and GSK690 for 72 hours. Shown is the number of genes (average of two biologic replicates) that are up (top) or down (bottom) regulated upon treatment with GSK690 or RN-1 by >2-fold in any of the three cell lines. The Venn diagram illustrates the similarity of gene expression changes caused by both agents. B, as in A, but shown are the genes that are significantly changed in expression (>2-fold; $P < 0.05$) upon RN-1 treatment in Kasumi-1, SKNO-1, and MV4-11 cells for 72 hours. The Venn diagram illustrates the similarity of RN-1-induced gene expression changes in each cell line. C, heatmap representation of gene expression changes in Kasumi-1, SKNO-1, and MV4-11 cells upon treatment with RN-1, GSK690, or GSK690* (compared with DMSO-treated controls). The data are presented as the average $\log_2$ fold change in expression of two biological replicates; the magnitude of the changes is indicated by a color scale (bottom), with shades of red indicating increase and shades of blue indicating decrease in expression. D, as in C, but only representing genes that are upregulated (>1.5-fold) in both Kasumi-1 and SKNO-1 cells upon treatment with RN-1, GSK690, or GSK690* for 72 hours. Significantly upregulated genes are indicated on the right. E, GSEA analysis of Kasumi-1 and SKNO-1 gene expression profiling data. F, the timing of KDM1A inhibitor-mediated induction of LY96 mRNA levels was determined. MV4-11 cells were treated with DMSO, RN-1 (1 μmol/L), and GSK690 (1 μmol/L) for indicated time points and mRNA levels determined using a QuantiGene assay. Data represent the mean of two independent experiments carried out in quadruplicate ±SEM. G, manual ChIP was performed for KDM1A (top) and H3K4me3 (bottom) in Kasumi-1 cells. KDM1A was found significantly enriched at the *LY96* promoter. H3K4me3 levels at the *LY96* TSS were substantially increased upon treatment with RN-1 and GSK690 (1 μmol/L each, treatment for 24 hours). ChIP with IgG was performed as a negative control. Data are presented as enrichment/total input ±SEM.

observe that the majority of genes whose expression changes upon KDM1A inhibitor treatment are upregulated in human AML cell lines. Importantly, KDM1A inhibitor-mediated gene expression changes were not only similar between biological replicates but also between the two completely different KDM1A inhibitor chemotypes, GSK690 and RN-1 (Fig. 4A and C). Moreover, GSK690*-mediated gene expression changes were similar but far weaker compared with those observed upon GSK690 and RN-1 treatment, consistent with it being a less potent KDM1A inhibitor. Collectively, our gene expression profiling data strongly suggest that compound-mediated transcriptional changes result from KDM1A inhibition.

Consistent with KDM1A's role in transcriptional repression, we identified a number of genes whose expression was robustly altered in both of the *RUNX1-RUNX1T1* translocation-containing AML cell lines (>4-fold change, $P < 0.05$; Fig. 4D and Supplementary Table S2). To identify gene sets whose coordinate expression was dependent upon KDM1A catalytic activity, we performed gene set enrichment analysis (GSEA) of transcriptional changes following treatment with the KDM1A inhibitors. The fact that similar GSEA results were obtained for KDM1A-controlled gene expression signatures in both Kasumi-1 and SKNO-1 cells underscores the similarity of the transcriptional changes caused by KDM1A inhibition across RUNX1-RUNX1T1 leukemias. Gene expression changes in our dataset were similar to changes induced by knockdown of known oncogenes such as *HOXA9*, *KRAS*, and *VEGF* (Supplementary Table S2). In particular, genes that are both upregulated and downregulated upon HOXA9 knockdown in leukemia cells (36) were significantly correlated with KDM1A inhibitor-induced gene expression changes (Fig. 4E). HOXA9 is a well-established oncogenic driver in AML (36, 37); our results suggest that while KDM1A inhibition does not directly impede on HOXA9 expression' however, molecular downstream consequences of KDM1A inhibitor treatment mimic to a certain extent loss of HOXA9 oncogenic signaling.

To gain insight into the kinetics of KDM1A inhibitor-mediated induction of gene expression, we focused on one of the most upregulated genes in our RNA-sequencing data, the lymphocyte-specific antigen *LY96*. Its expression was substantially induced as early as 4 hours after the addition of RN-1 or GSK690 (Fig. 4F). Maximal induction was achieved after 16 hours of treatment and persisted for at least 96 hours in the presence of compound. We determined by ChIP that KDM1A bound directly to the *LY96* promoter region and that H3K4me3, a modification specifically associated with active transcription, was significantly enriched at the *LY96* transcription start site (TSS) upon treatment with both RN-1 and GSK690 (Fig. 4G). Our data show that chromatin structural and transcriptional changes on KDM1A target genes precede phenotypic effects, which are usually not detected before 3 to 4 days of compound treatment.

KDM1A inhibitors evict KDM1A from chromatin

KDM1A inhibitors did not alter global levels of histone H3K4 and H3K9 di-methylation, even at concentrations that eventually affect cell viability (Supplementary Fig. S5A and S5B). Moreover, the levels of KDM1A and the integrity of the KDM1A-containing protein complex appeared to be unaffected by inhibitor treatment (Supplementary Fig. S5C). We reasoned that the molecular consequences of KDM1A inhibition are perhaps detectable at specific genomic locations, and thus performed ChIP and DNA sequencing (ChIP-seq) for KDM1A in Kasumi-1 and SKNO-1 cells in the absence or presence of the KDM1A inhibitors RN-1 and GSK690. Many KDM1A loci were occupied across all treatment conditions: 19,232 and 15,167 regions in Kasumi-1 and SKNO-1 cells, respectively. KDM1A binding at TSS was significantly above random but was also frequently observed in gene bodies and intergenic regions (Fig. 5A, top). Most high-confidence KDM1A-binding sites in one cell line were also observed in the other cell line (Fig. 5A, bottom). Although the majority of KDM1A genomic-binding sites remained unchanged upon KDM1A inhibitor treatment (Fig. 5B and Supplementary Fig. S6A), surprisingly, both irreversible and reversible inhibitors led to a marked loss of KDM1A occupancy at a number of genomic locations in both cell lines. (Fig. 5B and C and Supplementary Fig. S6B and S6C). Since KDM1A catalyzes the demethylation of mono- and di-methylated but not tri-methylated H3K4, we performed ChIP-seq to determine potential changes in local H3K4me2 levels on KDM1A target genes. Many KDM1A target genes such as *LY96*, *ID3*, *PI16*, *ACVR2A*, *KCTD12*, *MS4A4A*, *TMEM251*, *FGD6*, and *RGBM* showed substantial KDM1A loss or redistribution with concomitant increase of H3K4me2 levels upon inhibitor treatment in both cell lines (Fig. 5D and Supplementary Fig. S6C). KDM1A redistribution is exemplified at the *LY96* locus where the inhibitor-induced loss of KDM1A leads to a new KDM1A peak upstream of the original binding site in both cell lines (Fig. 5D, left). We confirmed by ChIP that RN-1 and GSK690 but not the weaker GSK690* isomer induced KDM1A loss on individual target genes including *LY96* (Supplementary Fig. S6D), indicating that it is indeed the inhibition of the enzyme that leads to KDM1A eviction. Interestingly, KDM1A occupied genes were not devoid of H3K4me2 and, depending on genomic context, showed H3K4me2 peak enrichments or a substantial broadening of the H3K4me2-positive area upon treatment with a KDM1A inhibitor. Increased H3K4me2 signal in the vicinity of KDM1A-binding sites was observed more frequently on loci that lose KDM1A upon RN-1 and GSK690 treatment. Comparison of KDM1A and H3K4me2 ChIP-seq data in Kasumi-1 cells shows that H3K4me2 gain is strongly correlated with loss of colocated KDM1A (Fig. 5E, bottom right quadrant). However, integrating the ChIP-seq and RNA-seq data, the expression of the majority of genes near KDM1A-binding sites remains unaffected upon inhibitor treatment, regardless of whether KDM1A is retained or displaced (Fig. 5F). This indicates that KDM1A inhibitors impact RUNX1-RUNX1T1 leukemia transcriptional profiles in a highly selective manner that is not necessarily predicted by KDM1A-binding patterns. On the other hand, upregulated genes are far more likely to have both loss of KDM1A and increase in H3K4me2 upon inhibitor treatment, compared with either downregulated genes or genes that are unchanged in expression (Fig. 5G). Genes with both, chromatin changes and transcriptional upregulation, are KDM1A target genes directly impacted by KDM1A inhibitors and represent a potentially valuable biomarker gene signature.

KDM1A inhibitor-mediated KDM1A chromatin eviction is rapid and precedes transcriptional response

Diminution of KDM1A occupancy by KDM1A inhibitors is unexpected with no previous precedent. Intrigued by the outcome of our ChIP-seq data, we further explored the impact of KDM1A inhibitors on KDM1A chromatin binding in RUNX1-RUNX1T1 leukemia models. Given that KDM1A inhibitors did not appear to

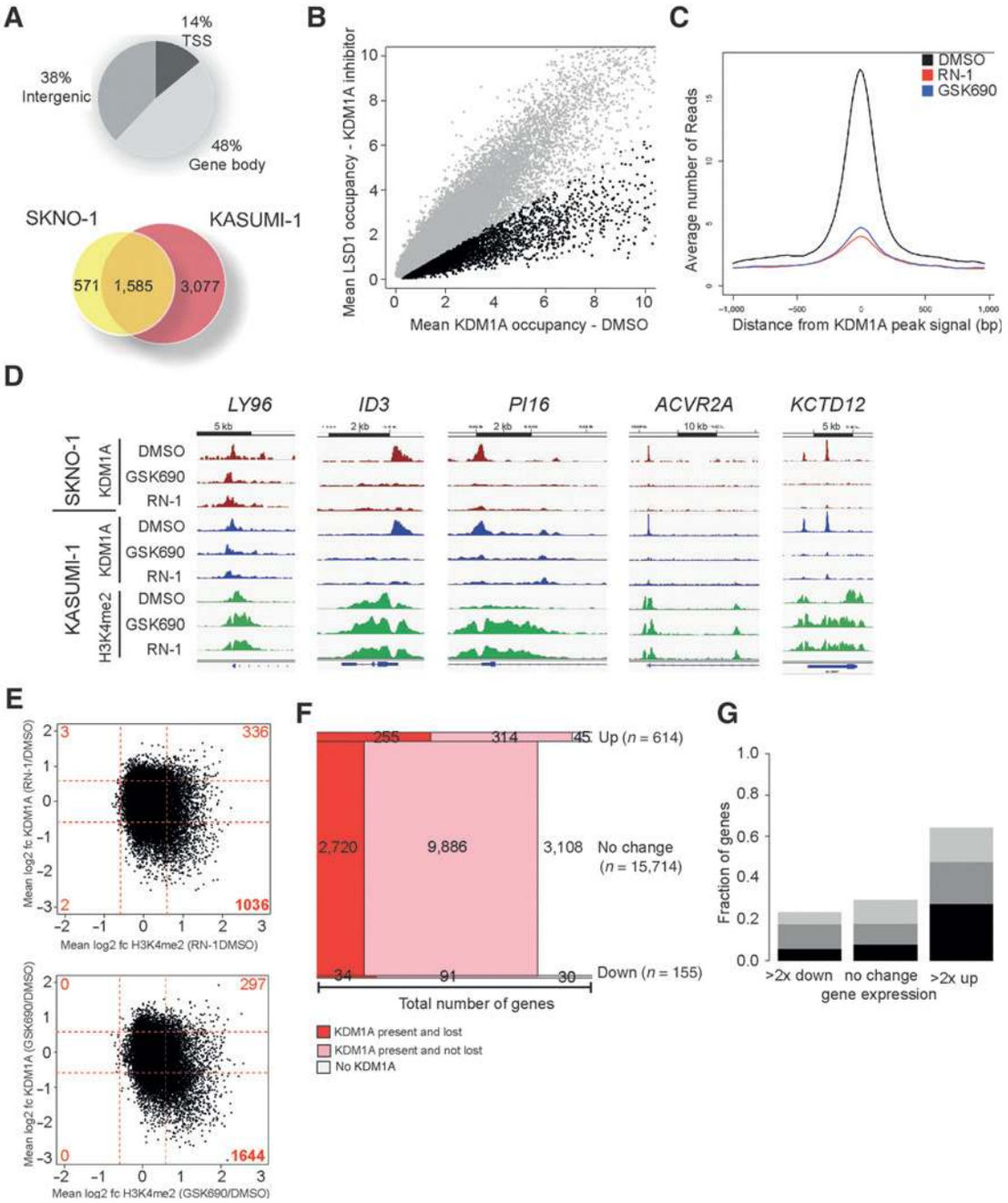

Figure 5.
KDM1A inhibitors affect KDM1A chromatin binding pattern. A, ChIP-seq was performed in Kasumi-1 and SKNO-1 cells in the presence of DMSO, RN-1 and GSK690 (1 μmol/L each) to determine KDM1A-binding sites. The Venn diagrams illustrate the overlap of high confidence ($-\log_{10}$ MACS $P > 250$) TSS proximal (−2,000/+2,000 bp) KDM1A-binding sites in both cell lines. B, signal (integrated normalized ChIP-seq fragments × 1000) at each KDM1A-binding site in Kasumi-1 cells treated with DMSO (*x*-axis) or KDM1A inhibitors (*y*-axis). C, average genome-wide KDM1A occupancy (−2,000, +2,000 interval around the center of each KDM1A region) in Kasumi-1 cells at genomic loci showing reduction upon treatment with the KDM1A inhibitors RN-1 and GSK690 for 72 hours compared with DMSO-treated controls. D, visualization of KDM1A and H3K4me2 profiles at selected KDM1A target genes in SKNO-1 (top) and Kasumi-1 (bottom) cells treated with DMSO, RN-1, and GSK690 for 72 hours. KDM1A occupancy is decreased and H3K4me2 levels are increased upon KDM1A inhibitor treatment. E, change of KDM1A and H3K4me2 occupancy in Kasumi-1 cells treated with DMSO and RN-1 (top) or DMSO and GSK690 (bottom). Data are presented as $\log_2$ fold change after adding a regularizing constant to integrated signal in each interval. Interval locations were calculated by MACS (see Materials and Methods for details). Dashed red lines indicate 1.5-fold change in mean signal. The number of loci that show (1) increase in H3K4me2 and decrease in KDM1A (lower right), (2) increase in H3K4me2 and KDM1A (upper right), (3) increase in KDM1A and decrease in H3K4me2 (upper left), and (4) decrease in KDM1A and H3K4me2 (lower left) are indicated. F, shown is a representation of all 16,483 expressed genes (expression signal >0 in any line) with respect to their KDM1A status in the absence or presence of KDM1A inhibitors and their respective expression changes upon KDM1A inhibitor treatment, with a 1.5-fold threshold. G, shown are the fractions of expressed genes >2-fold downregulated (total $n = 17$), unchanged ($n = 16{,}273$), or >2-fold upregulated ($n = 205$) that exhibit (1) KDM1A loss and H3K4me2 gain (black), (2) KDM1A loss only (dark gray), or (3) H3K4me2 gain (light gray) in Kasumi-1 cells upon KDM1A inhibitor treatment.

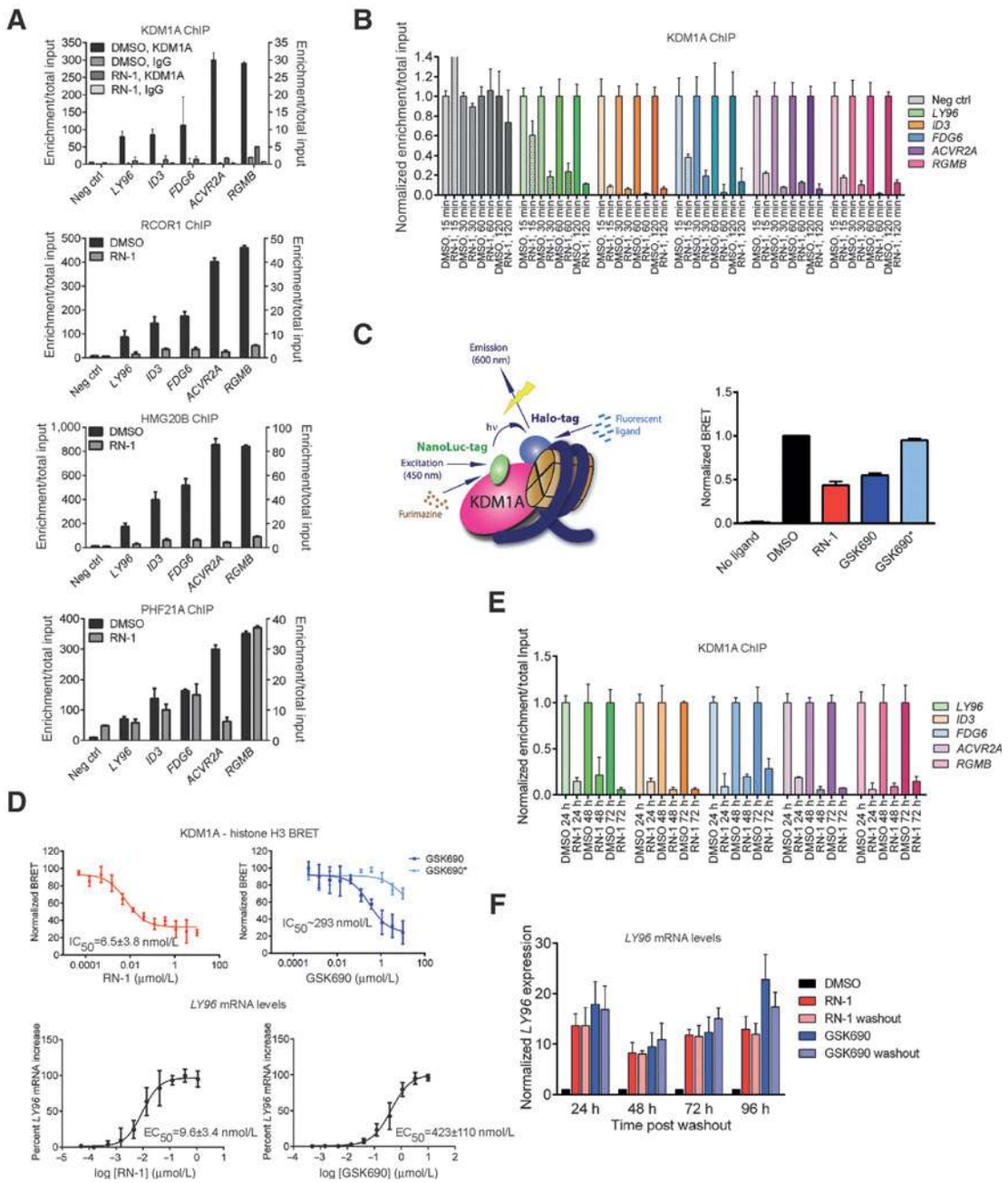

Figure 6.

KDM1A and its complex partners are rapidly evicted from chromatin upon KDM1A inhibitor treatment. A, RN-1 displaces KDM1A and KDM1A complex components from target genes. ChIP was performed in Kasumi-1 cells after 24 hours of treatment with DMSO or RN-1 (1 μmol/L). Data are presented as enrichment/total input ±SEM and are calculated from the average of PCR quadruplicates. B, inhibitor-mediated loss of KDM1A chromatin binding is rapid. ChIP was performed in Kasumi-1 cells after 15, 30, 60, and 120 minutes of treatment with DMSO or RN-1 (1 μmol/L). Data are presented as enrichment/total input ±SEM and are calculated from the average of PCR quadruplicates. KDM1A enrichment of treated samples is normalized to the corresponding ChIP of DMSO-treated samples. C, determination of inhibitor-induced loss of KDM1A binding to histone H3 in living cells by a NanoBRET assay. HEK293 cells were transfected with NanoLuc-KDM1A and HaloTag-H3 and DMSO or KDM1A inhibitor added 24 hours post-transfection. Relative NanoBRET signal was measured 24 hours after the addition of compounds. Data are presented as the mean of two independent experiments carried out in quadruplicate ±SEM. D, RN-1 (left) and GSK690 (right) displace KDM1A from histone H3 in a dose-dependent manner as measured by BRET as described in C. The ability of compounds to displace KDM1A (top) parallels their ability to induce KDM1A target gene expression (bottom). *LY96* mRNA levels were determined and normalized to *GAPDH* mRNA levels in MV4-11 cells using a Quantigene assay. Data represent the mean of two (top) and three (bottom) independent experiments carried out in triplicate ±SEM. E, KDM1A remains evicted from target genes 48 hours post RN-1 removal. Kasumi-1 cells were treated for 24 hours with DMSO or RN-1 (1 μmol/L). Data are presented as normalized enrichment/total input ±SEM and are calculated from the average of PCR quadruplicates normalized to each time points' respective DMSO control. F, KDM1A inhibitor treatment leads to prolonged *LY96* gene induction that is maintained after compound removal. MV4-11 cells were treated with DMSO, RN-1 (1 μmol/L), or GSK690 (1 μmol/L) for 24 hours, upon which cells were washed and cultured in fresh medium for additional 24, 48, 72, and 96 hours post compound removal. *LY96* mRNA levels were determined and normalized to *GAPDH* mRNA levels using a QuantiGene assay. Data represent the mean of two independent experiments carried out in quadruplicate ±SEM.

reduce cellular levels of KDM1A or disrupt the KDM1A-containing protein complex (Supplementary Fig. S5C), we examined how KDM1A inhibition affected the chromatin binding of complex components. Treatment with RN-1 effectively displaced KDM1A together with RCOR1 and HMG20B (Fig. 6A). In contrast, PHF21A occupancy was unaffected on all inspected KDM1A target genes with the exception of *ACVR2A*. KDM1A was largely displaced within an hour of compound treatment (Fig. 6B), and thus well before any increase in gene expression was detected (see for example Fig. 4F).

As an orthogonal approach to measure inhibitor-mediated loss of KDM1A from chromatin, HEK293T cells were transfected with plasmids expressing Halo-tagged histone isoform H3.1 and NanoLuciferase-tagged KDM1A and the physical proximity between these two proteins was monitored by bioluminescence resonance energy transfer (NanoBRET, Fig. 6C, left). RN-1 and GSK690 but not GSK690* reduced the BRET signal in the transfected cells (Fig. 6C, right), indicative of a partial ablation of the KDM1A:histone H3 interaction. Both chemotypes impacted the KDM1A interaction with histone H3 in a dose-dependent manner (Fig. 6D, top), which correlated well with their abilities to induce KDM1A target gene expression (Fig. 6D, bottom). KDM1A rebinding (Fig. 6D and Supplementary Fig. S6E) and restoration of gene silencing (Fig. 6F) were not observed post compound removal for at least 48 and 96 hours, respectively, suggesting that the molecular consequences of KDM1A inhibition are relatively long-lived.

KDM1A inhibitors combine with other agents for the treatment of AML

Given that KDM1A inhibitor single-agent activity was limited in some AML cell lines, we evaluated whether KDM1A inhibitors in combination with other agents achieve improved phenotypic responses. To explore potential combinatorial effects, we carried out two-dimensional dose titrations of both agents and measured in parallel cell viability for each unique combination of drug concentrations. Cell viability data were then subjected to various analysis methods to differentiate synergy from simple additive effects (details of synergy determination and analysis methods are described in the Supplementary Methods). Initially, we explored whether KDM1A inhibition would increase the efficacy of the standard of care agent in AML, cytarabine (Ara-C). Combining RN-1 and Ara-C was substantially more effective in reducing AML cell viability than either agent alone in a number of AML cell lines (Fig. 7A), indicative of synergy between these two agents. Synergy was detected preferentially in cell models that were less sensitive to either single agent (Fig. 7A, table on the right).

KDM1A inhibitors were previously shown to synergize with ATRA (25) as well as with histone deacetylase inhibitors (38), agents that modulate chromatin structure and transcriptional programs. ATRA alone had minimal effects on cell viability, but enhanced and accelerated the effects of RN-1 in a number of AML cell lines representing various AML subtypes (Fig. 7B). The impact on cell viability was achieved by a number of different ATRA and KDM1A inhibitor dose combinations, indicating substantial synergy as measured by Bliss independence volume (Fig. 7B, table on the right).

We and others have shown that small-molecule inhibitors of the histone methyltransferase EZH2 alter gene expression programs and are efficacious in non-Hodgkin lymphoma subtypes (39, 40). Recently, it was suggested that EZH2 inhibitors are also effective in the treatment of AML (41). Thus, the potential for KDM1A inhibitors to work in combination with EZH2 inhibitors was investigated. MOLM-13 cells were effectively killed by the EZH2-KDM1A inhibitor combination (Fig. 7C), showing remarkable synergy, regardless of the method used to calculate the combinatorial effects (Supplementary Fig. S7). Expanding these studies, combinatorial effects were evident in a number of additional leukemia cell line models (Fig. 7C, table on the right).

Collectively, these studies suggest that KDM1A inhibitors can be successfully combined with chemotherapeutic and targeted agents, and that combinations may be an effective therapeutic strategy in a clinical setting.

Discussion

We have shown here that KDM1A inhibition is broadly efficacious across cell lines representing the various AML subtypes. While our manuscript was in preparation, small cell lung cancers of the neuroendocrine subtype were reported to be dependent on KDM1A (42). In this study, irreversible KDM1A inhibitors were used across a large cancer cell panel and broad responses in AML were noted, in agreement with our data. In addition to AML, we also identified CML and T-ALL as potential indications for KDM1A inhibitors. A number of AML cell lines showed less than 100% cell killing. In such cases, a cell subpopulation is effectively eliminated; however, growth of entire populations appeared critically affected by KDM1A inhibitors when evaluated in colony formation assays (Supplementary Fig. S3). Clonal architecture in AML gives rise to functional heterogeneity that impacts disease aggressiveness and progression (43). AML cell lines may recapitulate some level of heterogeneity, which could affect in some instances their sensitivity to KDM1A inhibitors. Future experimentation will be required to explore the molecular characteristics of the resistant cell subpopulation after KDM1A inhibitor treatment and compare their engraftment potential with that of the parental AML cell line. Our studies also suggest that the addition of a second therapeutic agent in combination with KDM1A inhibitors may be a useful strategy to achieve more complete responses in AML.

In depth examination of leukemia models that are defined by the presence of *RUNX1-RUNX1T1* translocations provided evidence that KDM1A inhibitors effectively suppress *in vitro* and *in vivo* growth of this leukemia subtype. *RUNX1-RUNX1T1* leukemias belong to a larger, heterogeneous subgroup termed core binding factor (CBF) leukemias. The core binding factor protein complex contains multiple transcription factors that are required for normal hematopoietic development (44). Genomic aberrations in any of the genes encoding for CBF components are associated with malignant transformation and promote AML (45). CBF leukemias include *RUNX1* mutations, *t*(8;21) and inv(16) translocations, the latter of which fuses core binding factor beta (*CBFB*) to the *MYH11* gene. ME-1 cells harbor a *CBFB-MYH11* translocation and were identified as KDM1A inhibitor-responsive in the AML cell panel (Fig. 1A). These data support the idea of broad KDM1A dependencies in CBF leukemias and future studies, especially those exploring primary samples, may provide clarification about the scope of KDM1A inhibitor response in CBF leukemias.

Transcriptional profiling in *RUNX1-RUNX1T1* cell models provided strong support for a role of the KDM1A in transcriptional repression, with little of the transcriptional activation

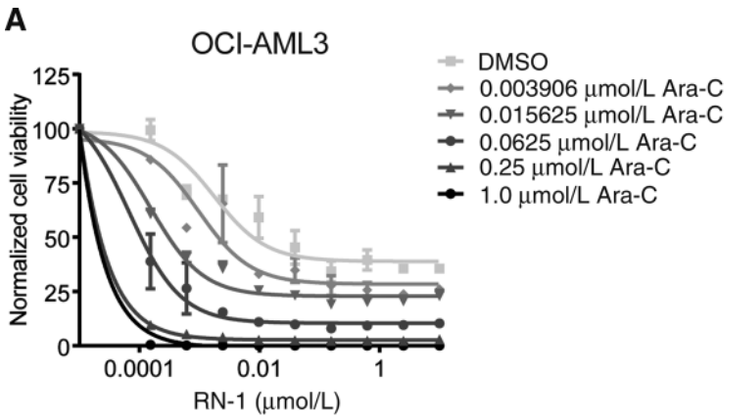

Cell line	RN-1 GI_{50} (μmol/L)	Ara-C GI_{50} (μmol/L)	Synergy score 0 1250 2,500
OCI-AML5	>10	>1	
MOLM-13	7.8	>1	
OCI-AML3	>10	>1	
SKM-1	>10	>1	
NOMO-1	>10	>1	
HL-60	0.014	>1	
MV4-11	0.017	>1	
Kasumi-1	0.046	0.03	
SKNO-1	0.01	0.03	
RS4;11	>10	0.004	

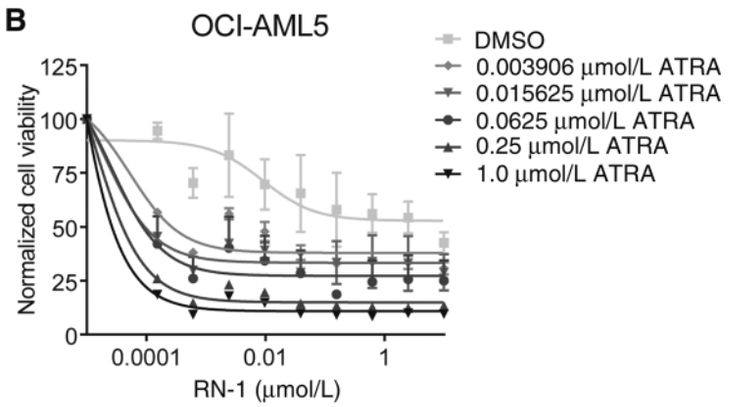

Cell line	RN-1 GI_{50} (μmol/L)	ATRA GI_{50} (μmol/L)	Synergy score 0 900 1,800
SKM-1	>10	>1	
SKNO-1	0.01	>1	
OCI-AML5	>10	>1	
THP-1	>10	>1	
NOMO-1	>10	>1	
MV4-11	0.017	0.05	
OCI-AML2	0.038	0.04	
MOLM-13	7.8	>1	
Kasumi-1	0.046	>1	

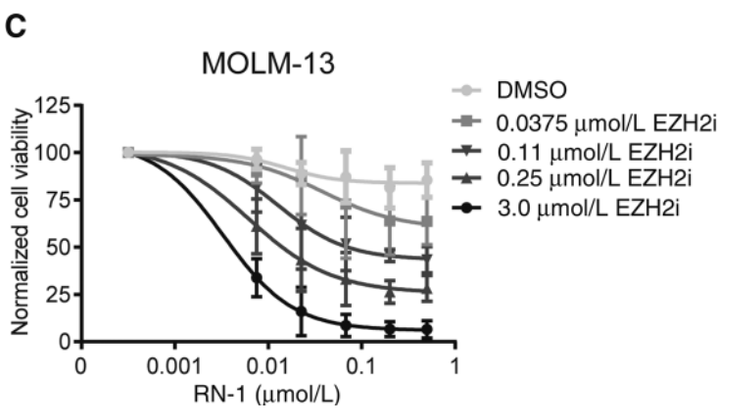

Cell line	RN-1 GI_{50} (μmol/L)	CPI-169 GI_{50} (μmol/L)	Synergy score 0 175 350
MOLM-13	>0.5	>3	
MV4-11	0.017	0.15	
RPMI-8402	>0.5	>3	
SKM-1	>0.5	>3	
NOMO-1	>0.5	>3	
KU812F	0.009	1.32	
OCI-AML2	0.038	3	
KASUMI-1*	0.046	>3	
SET2	0.02	>3	
SKNO-1	0.01	0.3	

Figure 7.
KDM1A inhibition shows synergy with other therapeutic agents. A, left panel shows RN-1 and Ara-C combination in OCI-AML5 cells, which displayed the greatest synergy of all tested cell lines as indicated in the table to the right. Shown in the table are the GI_{50} values for each agent as well as the Bliss independence volume calculated from the two-dimensional dose titration cell viability data. All data are represented as the mean of duplicate experiments ±SEM. Cells were treated with both agents at the doses indicated for 8 days, with passaging into fresh drug at day 4. B, RN-1 and ATRA combination in SKM-1 cells. Cells were treated with both agents at the doses indicated for 4 days. GI_{50} values and synergy scores are summarized in the table to the right. C, RN-1 and EZH2 inhibitor combination in MOLM-13 cells. The EZH2 inhibitor CPI-169 showed strong synergy when dosed in combination with RN-1 over a 12-day period. Cells were passaged and compounds were renewed every 4 days. Table summarizes KDM1A and EZH2 inhibitor single agent and combinatorial activities in a number of AML and T-ALL cell lines.

reported previously (10, 46). Though, it is possible that the coactivator role rests on a scaffolding function of KDM1A that may only be perturbed by protein depletion. This would be consistent with a study in which many more genes were down-regulated rather than upregulated when Kdm1a was diminished by RNAi in a murine Mll-Af9–driven AML model (24). Clearly, our study indicates that KDM1A inhibitors elicit mostly increases in gene expression. In fact, both inhibitor chemotypes cause very

similar changes in gene expression, further substantiating the argument that these effects are caused by compound on-target activity and that KDM1A inhibition largely perturbs the KDM1A corepressor function. The "signature" of genes altered by KDM1A inhibitor treatment correlated well with gene sets that were altered in human MLL-rearranged AML models upon knockdown of the oncogenic transcription factor HOXA9 (36). Although we did not detect downregulation of *HOXA9* or its cofactors *MEIS1* and *PBX3*, nor the transcription factor *MEF2C*, we see a striking correlation of genes altered by KDM1A inhibitors with both genes downregulated and upregulated by HOXA9 knockdown. Engineered overexpression of HOXA9 in *RUNX1-RUNX1T1* AML cell lines had no effect on their sensitivity to KDM1A inhibition (data not shown), suggesting that the common effects on transcriptional programs are not mediated directly by the action of HOXA9 alone. Actually, *HOXA9* and *MEIS1* expression levels are relatively low in primary *RUNX1-RUNX1T1* leukemias (47), and thus not likely to confer a proliferative advantage in this AML subtype. This is consistent with the concept that transcriptional signatures in different leukemia subtypes, categorized on the basis of primary genomic aberrations, are distinct from each other (48). However, our data suggest that RUNX1-rearranged and MLL-rearranged leukemias may converge on similar downstream oncogenic pathways that are impacted by KDM1A inhibition. Functional consequences of KDM1A inhibition in RUNX1-RUNX1T1 AML models include both induction of differentiation and cell death. Interestingly, KDM1A inhibitors induce the expression of the proapoptotic factors TNFSF10 (TRAIL, APO2L) and TNF (TNFα) in Kasumi-1 and SKNO-1 cells. TNFSF10 is a potent inducer of the extrinsic pathway of programmed cell death and was shown to induce apoptosis in the context of *RUNX1-RUNX1T1* translocations under hypoxic conditions (49). Perhaps TNFSF10 or TNF induction contributes to the repertoire by which KDM1A inhibitors affect the viability of *RUNX1-RUNX1T1* leukemias.

KDM1A inhibitor mediated eviction of KDM1A from certain genomic locations was an unexpected finding. Since both inhibitor chemotypes produced very similar results, it is likely that this is a mechanism-based molecular consequence of KDM1A inhibition rather than a compound-specific phenomenon. The KDM1A protein complex has several "molecular handles" to retain chromatin association, and thus one would not predict that the binding of the KDM1A active site to the histone H3 N-terminal region is the dominant factor controlling KDM1A chromatin residency. ChIP-seq and BRET assay data suggest that loss of KDM1A upon inhibitor treatment is a context-specific phenomenon that does not globally affect KDM1A chromatin association. A recent study of KDM1A-binding sites in small cell lung cancer models upon KDM1A inhibitor treatment did not report any changes in chromatin association (42). Our data support the concept that inhibitor-mediated loss of KDM1A results in more pronounced changes in H3K4me2 levels as well as transcriptional activation as compared with mere KDM1A inhibition. It will be interesting to resolve in future studies whether the therapeutic impact of KDM1A inhibitors in AML stems from the inhibition of KDM1A catalytic activity or the context-dependent KDM1A complex displacement.

KDM1A inhibitors are among an increasing number of approaches targeting chromatin regulators that have recently entered clinical trials. Our data suggest that broad KDM1A dependencies exist in human AML, with CBF leukemias being of potential interest from a clinical perspective. Despite the requirement of KDM1A for normal hematopoiesis, KDM1A inhibitors exhibit a clear window of opportunity in an AML therapeutic setting. Our finding that both irreversible and reversible KDM1A inhibitor-mediated induction of gene expression is prolonged for multiple days after compound removal is interesting from a therapeutic standpoint. This modality having entered the clinic will spur the interest to answer questions regarding the extent of the therapeutic window and the optimal dosing paradigm in the near term.

Disclosure of Potential Conflicts of Interest

B.M. Bryant has ownership interest (including patents) in Constellation Pharmaceuticals. No potential conflicts of interest were disclosed by the other authors.

Authors' Contributions

Conception and design: T. O'Brien, S. Magnuson, P. Trojer
Development of methodology: J.P. McGrath, S. Balasubramanian, S. Odate, B.M. Bryant
Acquisition of data (provided animals, acquired and managed patients, provided facilities, etc.): J.P. McGrath, K.E. Williamson, S. Balasubramanian, S. Odate, S. Arora, T.M. Edwards, S. Magnuson, D.L. Daniels
Analysis and interpretation of data (e.g., statistical analysis, biostatistics, computational analysis): J.P. McGrath, K.E. Williamson, S. Balasubramanian, S. Odate, S. Arora, C. Hatton, D. Stokoe, D.L. Daniels, B.M. Bryant, P. Trojer
Writing, review, and/or revision of the manuscript: J.P. McGrath, K.E. Williamson, S. Balasubramanian, S. Arora, T. O'Brien, S. Magnuson, D.L. Daniels, B.M. Bryant, P. Trojer
Administrative, technical, or material support (i.e., reporting or organizing data, constructing databases): S. Balasubramanian, B.M. Bryant, P. Trojer
Study supervision: P. Trojer

Acknowledgments

The authors thank Dr. Fei Lan for reagent support.

The costs of publication of this article were defrayed in part by the payment of page charges. This article must therefore be hereby marked *advertisement* in accordance with 18 U.S.C. Section 1734 solely to indicate this fact.

Received August 22, 2015; revised December 1, 2015; accepted December 22, 2015; published OnlineFirst February 2, 2016.

References

1. McGrath J, Trojer P. Targeting histone lysine methylation in cancer. Pharmacol Ther 2015;150:1–22.
2. Zack TI, Schumacher SE, Carter SL, Cherniack AD, Saksena G, Tabak B, et al. Pan-cancer patterns of somatic copy number alteration. Nat Genet 2013;45:1134–40.
3. Lawrence MS, Stojanov P, Mermel CH, Robinson JT, Garraway LA, Golub TR, et al. Discovery and saturation analysis of cancer genes across 21 tumour types. Nature 2014;505:495–501.
4. Kandoth C, McLellan MD, Vandin F, Ye K, Niu B, Lu C, et al. Mutational landscape and significance across 12 major cancer types. Nature 2013;502:333–9.
5. Gonzalez-Perez A, Jene-Sanz A, Lopez-Bigas N. The mutational landscape of chromatin regulatory factors across 4,623 tumor samples. Genome Biol 2013;14:r106.
6. Jones S, Stransky N, McCord CL, Cerami E, Lagowski J, Kelly D, et al. Genomic analyses of gynaecologic carcinosarcomas reveal frequent

mutations in chromatin remodelling genes. Nat Commun 2014;5: 5006.
7. Copeland RA, Moyer MP, Richon VM. Targeting genetic alterations in protein methyltransferases for personalized cancer therapeutics. Oncogene 2013;32:939–46.
8. Thinnes CC, England KS, Kawamura A, Chowdhury R, Schofield CJ, Hopkinson RJ. Targeting histone lysine demethylases - Progress, challenges, and the future. Biochim Biophys Acta 2014;1839:1416–32.
9. Shi Y, Lan F, Matson C, Mulligan P, Whetstine JR, Cole PA, et al. Histone demethylation mediated by the nuclear amine oxidase homolog LSD1. Cell 2004;119:941–53.
10. Metzger E, Wissmann M, Yin N, Muller JM, Schneider R, Peters AH, et al. LSD1 demethylates repressive histone marks to promote androgen-receptor-dependent transcription. Nature 2005;437:436–9.
11. Laurent B, Ruitu L, Murn J, Hempel K, Ferrao R, Xiang Y, et al. A specific LSD1/KDM1A isoform regulates neuronal differentiation through H3K9 demethylation. Mol Cell 2015;57:957–70.
12. Lee MG, Wynder C, Cooch N, Shiekhattar R. An essential role for CoREST in nucleosomal histone 3 lysine 4 demethylation. Nature 2005;437:432–5.
13. Shi YJ, Matson C, Lan F, Iwase S, Baba T, Shi Y. Regulation of LSD1 histone demethylase activity by its associated factors. Mol Cell 2005;19:857–64.
14. Lan F, Collins RE, De Cegli R, Alpatov R, Horton JR, Shi X, et al. Recognition of unmethylated histone H3 lysine 4 links BHC80 to LSD1-mediated gene repression. Nature 2007;448:718–22.
15. Marmorstein LY, Kinev AV, Chan GK, Bochar DA, Beniya H, Epstein JA, et al. A human BRCA2 complex containing a structural DNA binding component influences cell cycle progression. Cell 2001;104:247–57.
16. Whyte WA, Bilodeau S, Orlando DA, Hoke HA, Frampton GM, Foster CT, et al. Enhancer decommissioning by LSD1 during embryonic stem cell differentiation. Nature 2012;482:221–5.
17. Wang J, Hevi S, Kurash JK, Lei H, Gay F, Bajko J, et al. The lysine demethylase LSD1 (KDM1) is required for maintenance of global DNA methylation. Nat Genet 2009;41:125–9.
18. Foster CT, Dovey OM, Lezina L, Luo JL, Gant TW, Barlev N, et al. Lysine-specific demethylase 1 regulates the embryonic transcriptome and CoREST stability. Mol Cell Biol 2010;30:4851–63.
19. Kerenyi MA, Shao Z, Hsu YJ, Guo G, Luc S, O'Brien K, et al. Histone demethylase Lsd1 represses hematopoietic stem and progenitor cell signatures during blood cell maturation. Elife 2013;2:e00633.
20. Rhodes DR, Kalyana-Sundaram S, Mahavisno V, Varambally R, Yu J, Briggs BB, et al. Oncomine 3.0: genes, pathways, and networks in a collection of 18,000 cancer gene expression profiles. Neoplasia 2007;9:166–80.
21. Radich JP, Dai H, Mao M, Oehler V, Schelter J, Druker B, et al. Gene expression changes associated with progression and response in chronic myeloid leukemia. Proc Natl Acad Sci U S A 2006;103:2794–9.
22. Niebel D, Kirfel J, Janzen V, Holler T, Majores M, Gutgemann I. Lysine-specific demethylase 1 (LSD1) in hematopoietic and lymphoid neoplasms. Blood 2014;124:151–2.
23. Goardon N, Marchi E, Atzberger A, Quek L, Schuh A, Soneji S, et al. Coexistence of LMPP-like and GMP-like leukemia stem cells in acute myeloid leukemia. Cancer Cell 2011;19:138–52.
24. Harris WJ, Huang X, Lynch JT, Spencer GJ, Hitchin JR, Li Y, et al. The histone demethylase KDM1A sustains the oncogenic potential of MLL-AF9 leukemia stem cells. Cancer Cell 2012;21:473–87.
25. Schenk T, Chen WC, Gollner S, Howell L, Jin L, Hebestreit K, et al. Inhibition of the LSD1 (KDM1A) demethylase reactivates the all-trans-retinoic acid differentiation pathway in acute myeloid leukemia. Nat Med 2012;18:605–11.
26. Kruger RG, Mohammad H, Smitheman K, Cusan M, Liu Y, Pappalardi M, et al. Inhibition of LSD1 as a therapeutic strategy for the treatment of acute myeloid leukemia. Blood 2013;122:3964–64.
27. Bradley WD, Arora S, Busby J, Balasubramanian S, Gehling VS, Nasveschuk CG, et al. EZH2 inhibitor efficacy in non-Hodgkin's lymphoma does not require suppression of H3K27 monomethylation. Chem Biol 2014;21: 1463–75.
28. Neelamegam R, Ricq EL, Malvaez M, Patnaik D, Norton S, Carlin SM, et al. Brain-penetrant LSD1 inhibitors can block memory consolidation. ACS Chem Neurosci 2012;3:120–28.
29. Martinez Molina D, Jafari R, Ignatushchenko M, Seki T, Larsson EA, Dan C, et al. Monitoring drug target engagement in cells and tissues using the cellular thermal shift assay. Science 2013;341:84–7.
30. Dhanak D. Drugging the cancer epigenome. Proceedings of te h104th Annual Meeting of the American Association for Cancer Research. [abstract]. In: Proceedings of the 104th AACR Annual Meeting 2015; 2015 April 18–25; Philadelphia, PA. Washington, DC: AACR; 2015.
31. Westendorf JJ, Yamamoto CM, Lenny N, Downing JR, Selsted ME, Hiebert SW. The t(8;21) fusion product, AML-1-ETO, associates with C/EBP-alpha, inhibits C/EBP-alpha-dependent transcription, and blocks granulocytic differentiation. Mol Cell Biol 1998;18:322–33.
32. Mulloy JC, Cammenga J, MacKenzie KL, Berguido FJ, Moore MA, Nimer SD. The AML1-ETO fusion protein promotes the expansion of human hematopoietic stem cells. Blood 2002;99:15–23.
33. Martinez N, Drescher B, Riehle H, Cullmann C, Vornlocher HP, Ganser A, et al. The oncogenic fusion protein RUNX1-CBFA2T1 supports proliferation and inhibits senescence in t(8;21)-positive leukaemic cells. BMC Cancer 2004;4:44.
34. Mitelman F, Heim S. Quantitative acute leukemia cytogenetics. Genes Chromosomes Cancer 1992;5:57–66.
35. Lynch JT, Cockerill MJ, Hitchin JR, Wiseman DH, Somervaille TC. CD86 expression as a surrogate cellular biomarker for pharmacological inhibition of the histone demethylase lysine-specific demethylase 1. Anal Biochem 2013;442:104–6.
36. Faber J, Krivtsov AV, Stubbs MC, Wright R, Davis TN, van den Heuvel-Eibrink M, et al. HOXA9 is required for survival in human MLL-rearranged acute leukemias. Blood 2009;113:2375–85.
37. Zeisig BB, Milne T, Garcia-Cuellar MP, Schreiner S, Martin ME, Fuchs U, et al. Hoxa9 and Meis1 are key targets for MLL-ENL-mediated cellular immortalization. Mol Cell Biol 2004;24:617–28.
38. Fiskus W, Sharma S, Shah B, Portier BP, Devaraj SG, Liu K, et al. Highly effective combination of LSD1 (KDM1A) antagonist and pan-histone deacetylase inhibitor against human AML cells. Leukemia 2014;28: 2155–64.
39. Garapaty-Rao S, Nasveschuk C, Gagnon A, Chan EY, Sandy P, Busby J, et al. Identification of EZH2 and EZH1 small molecule inhibitors with selective impact on diffuse large B cell lymphoma cell growth. Chem Biol 2013;20:1329–39.
40. Knutson SK, Kawano S, Minoshima Y, Warholic NM, Huang KC, Xiao Y, et al. Selective inhibition of EZH2 by EPZ-6438 leads to potent antitumor activity in EZH2-mutant non-Hodgkin lymphoma. Mol Cancer Ther 2014;13:842–54.
41. Xu B, On DM, Ma A, Parton T, Konze KD, Pattenden SG, et al. Selective inhibition of EZH2 and EZH1 enzymatic activity by a small molecule suppresses MLL-rearranged leukemia. Blood 2015;125:346–57.
42. Mohammad HP, Smitheman KN, Kamat CD, Soong D, Federowicz KE, Van Aller GS, et al. A DNA hypomethylation signature predicts antitumor activity of LSD1 inhibitors in SCLC. Cancer Cell 2015; 28:57–69.
43. Klco JM, Spencer DH, Miller CA, Griffith M, Lamprecht TL, O'Laughlin M, et al. Functional heterogeneity of genetically defined subclones in acute myeloid leukemia. Cancer Cell 2014;25:379–92.
44. de Bruijn MF, Speck NA. Core-binding factors in hematopoiesis and immune function. Oncogene 2004;23:4238–48.
45. Sinha C, Cunningham LC, Liu PP. Core binding factor acute myeloid leukemia: new prognostic categories and therapeutic opportunities. Semin Hematol 2015;52:215–22.
46. Wang J, Scully K, Zhu X, Cai L, Zhang J, Prefontaine GG, et al. Opposing LSD1 complexes function in developmental gene activation and repression programmes. Nature 2007;446:882–7.
47. Lasa A, Carnicer MJ, Aventin A, Estivill C, Brunet S, Sierra J, et al. MEIS 1 expression is downregulated through promoter hypermethylation in AML1-ETO acute myeloid leukemias. Leukemia 2004;18:1231–7.
48. Andersson A, Eden P, Lindgren D, Nilsson J, Lassen C, Heldrup J, et al. Gene expression profiling of leukemic cell lines reveals conserved molecular signatures among subtypes with specific genetic aberrations. Leukemia 2005;19:1042–50.
49. Barbetti V, Tusa I, Cipolleschi MG, Rovida E, Dello Sbarba P. AML1/ETO sensitizes via TRAIL acute myeloid leukemia cells to the pro-apoptotic effects of hypoxia. Cell Death Dis 2013;4:e536.